Computational Materials Science 119 (2016) 120–129

Contents lists available at ScienceDirect

Computational Materials Science

journal homepage: www.elsevier.com/locate/commatsci

Influence of alloying elements upon the theoretical tensile strength of Ni-based model superalloy: γ-Ni/γ'-Ni_3Al multilayer

Xiao-Xia Wu [a,b], Chong-Yu Wang [a,c,*]

[a] Central Iron and Steel Research Institute, Beijing 100081, China
[b] School of Mathematics, Physics and Biological Engineering, Inner Mongolia University of Science and Technology, Baotou 041010, China
[c] Department of Physics, Tsinghua University, Beijing 100084, China

ARTICLE INFO

Article history:
Received 1 October 2015
Received in revised form 31 March 2016
Accepted 2 April 2016
Available online 18 April 2016

Keywords:
γ-Ni/γ'-Ni_3Al multilayer
Theoretical tensile strength
Alloying element
First principles

ABSTRACT

The theoretical tensile strength of Ni-based model superalloys was investigated by density functional theory calculations. The superalloy was modeled as a γ-Ni/γ'-Ni_3Al multilayer, and the strengthening effect induced by alloying elements X (X = Re, Ru, Cr, Mo, W, or Ta) close to the γ/γ' interface was investigated. Theoretical calculations show that the tensile strength of the model superalloy is ~1 GPa higher than that of the γ'-Ni_3Al phase, although the critical strain is ~38% lower than that of the pure γ'-Ni_3Al phase. Except for Ta, doping at the Al site of the γ-Ni/γ'-Ni_3Al interface significantly increases the theoretical tensile strength (>7%) or critical strain (>10%) of the γ-Ni/γ'-Ni_3Al multilayer. Local atomic disorder is observed in the Ni–Al sublayer of the γ'-Ni_3Al block of the superalloy, wherein the Ni–Al atomic layer decomposes into an Al layer and a Ni layer when the strain exceeds a critical value. The charge density difference and partial density of states provide further insight into the changes of chemical bonds and charge redistribution during the tensile process. Charge transfer from Al to Ni in the γ'-Ni_3Al precipitate of the superalloy could account for its higher tensile strength than the single γ' phase. Moreover, covalent-like Ni–X bonds inhibit deformation of the system, resulting in tensile strengthening of doped γ-Ni/γ'-Ni_3Al multilayers.

1. Introduction

Because of their excellent high-temperature mechanical properties, Ni-based single-crystal superalloys are widely used for blade applications in aircraft jet engines and land-based power generators [1–3]. The superalloy is composed of a precipitate in the cubic γ' phase ($L1_2$, ordered face-centered cubic (fcc), Ni_3Al) and a matrix in the γ phase (disordered fcc, Ni-based solid solution). Experiments and theoretical calculations indicate that the γ-Ni and γ'-Ni_3Al interphase boundary is coherent with a simple cubic–cubic [001]||[001] relation [4,5]. After short exposure to service conditions, the microstructure of the superalloy changes into a morphology known as directional coarsening (or rafting), which is a lamellar structure composed of alternating γ-Ni and γ'-Ni_3Al phases [6,7]. The rafting structure effectively impedes movement of dislocations near the γ/γ' interfaces by a variety of mechanisms, and it is considered to be a hardening process that remarkably enhances the creep strength of Ni-based superalloys [8–10]. The addition of platinum metals and refractory elements such as Co, Cr, Mo, Re, Ru, Ta, and W greatly improves the overall performance of superalloys, especially the high-temperature creep rupture strength, thermal fatigue resistance, and oxidation resistance. Recently, numerous experimental and theoretical studies have revealed that factors such as the interface, dislocations, cracks, and the synergistic effect of elements [11–16] have important effects on the mechanical properties of superalloys. However, it is still not completely understood how these factors contribute to the mechanical properties of metallic structure materials.

The theoretical strength (or ideal strength) is a measure of maximum strength of an ideal single crystal. It is an essential parameter to understand the deformation mechanisms of materials, and therefore it has attracted considerable attention both experimentally and theoretically. The ideal strengths of various crystals have been obtained by nanoindentation experiments [17–20] owing to the recent development of nanoindentation techniques and material processing techniques to form nano- or microcrystalline metals with greatly reduced densities of movable dislocations in each grain. Motivated by these experimental results, many computational studies have been performed to evaluate the ideal strength,

* Corresponding author at: Department of Physics, Tsinghua University, Beijing 100084, China. Tel.: +86 10 62781141.
E-mail addresses: wuxiaoxia19800927@163.com (X.-X. Wu), cywang@mail.tsinghua.edu.cn (C.-Y. Wang).

http://dx.doi.org/10.1016/j.commatsci.2016.04.001
0927-0256/

including molecular dynamics [21] and an *ab initio* approaches [22–25]. Ogata et al. [22] analyzed the stress–strain responses of 22 simple metals and ceramics using density functional theory (DFT) to determine the maximum shear strain that a homogeneous crystal can withstand. They refer to this as the shearability, and found that the shearability of the metal is correlated with the degree of valence charge localization and directional bonding. Liu et al. [23] used a first-principles total-energy method to systematically investigate the theoretical tensile and shear strength of fcc Ni, and they analyzed the charge distribution to understand the intrinsic mechanical properties of Ni. Wang and Wang [24] performed first-principles calculations to investigate the effect of Re on the ideal strength of γ'-Ni_3Al under tensile uniaxial loads and ideal shear stresses. They found that the addition of Re considerably improved both the tensile and shear strength of Ni_3Al. In addition, electronic structure analysis suggested that the covalent-like Re–Ni bond would effectively resist deformation of Ni_3Al and lead to a higher strength.

For Ni-based superalloys, the tensile strength of each phase gives an indication of the mechanical properties. However, the structure and properties of the γ/γ' interface and dopants at the interface affect the creep strength or creep rupture life of Ni-based single-crystal superalloys subjected to stress at elevated temperatures [26–32]. For example, Gong et al. [26] investigated the strengthening effects induced by alloying elements at the Ni/Ni_3Al interface in terms of Griffith's equation using DFT. Chen et al. [12] used the DMol molecular orbital package, which performs first-principles calculations based on DFT, to calculate the electronic structures and bonding characteristics of the Ni/Ni_3Al interface using a cluster model. Peng et al. [13] investigated the effects of Re, B, P, and S on the interface properties of Ni/Ni_3Al. They found that Re and B improve the interfacial fracture strength, while P and S have a deleterious effect. However, these studies generally focused on either the site preference of dopants or energetic analysis combined with electronic structures, which may not be sufficient to understand the interfacial adhesion strength and the overall tensile strength of the superalloy. Therefore, it is important to carefully investigate the stress–strain relationship and the ideal strength of the γ-Ni/γ'-Ni_3Al multilayer model system to obtain a more complete understanding of the mechanical behavior of Ni-based superalloys.

In this study, according to the stress–strain relationships determined from first-principles calculations, we investigate the influences of the thickness of the Ni/Ni_3Al multilayer and doping with X (X = Re, Ru, Cr, Mo, W, Ta) on the theoretical tensile strength. In addition, we perform detailed analyses of local deformation, the electronic structure of the Ni/Ni_3Al coherent multilayer, and the electronic mechanism of doping at the interface underlying the strengthening effects to provide deeper insight into the failure characteristics of the interface and the strengthening effects owing to doping of the alloying elements.

2. Model and computational methods

For the γ-Ni/γ'-Ni_3Al multilayer, we used the standard approach to investigate the theoretical tensile strength of crystalline solids from DFT calculations [33,34]. The first step was to determine the equilibrium crystallographic structure and lattice parameters of the alloys. A uniaxial tensile test was then incrementally applied along a specific crystallographic direction to mimic a certain tensile stress (σ). The direction of the uniaxial tensile strain was along the [001] direction, while the atomic (001) plane perpendicular to the applied strain was simultaneously relaxed until the stress components in these directions disappeared. All of the internal degrees of freedom of each atom were fully relaxed until the atoms reached their equilibrium at each strain stage.

The total energies were calculated using DFT implemented in the Vienna *Ab initio* Simulation Package [35], and the electron–ion interaction was treated by the projector augmented-wave method [36]. The generalized gradient approximation with the parameterization of Perdew, Burke, and Ernzerhof [37] was used to evaluate exchange–correlation effects, and the electronic wave functions were expanded in plane waves up to a cutoff kinetic energy of 400 eV. To ensure the accuracy of the self-consistent calculation, an energy convergence criterion of 10^{-5} eV was used throughout the study. The corresponding $10 \times 10 \times 2$ k-point mesh, which was chosen with a regular Monkhorst–Pack scheme [11], was used in the calculation according to the size of the supercell, wherein all of the atomic positions in the supercell were relaxed until the quantum–mechanical Hellmann–Feynman forces on all atoms were less than 0.02 eV/Å. A nonspin polarized calculation was performed to investigate the mechanical properties of the Ni-based superalloys because the service temperature is well above the Curie temperature.

Periodic sandwich structures of the γ-Ni[001]||γ'-Ni_3Al[001] multilayer were used to model the Ni-based superalloys, as shown in Fig. 1. Fig. 1 shows the conventional unit cells of fcc-Ni (γ-Ni) (Fig. 1(a)) and $L1_2$-Ni_3Al (γ'-Ni_3Al) (Fig. 1(b)), as well as the undoped model composed of 8(γ-Ni) + 8(γ'-Ni_3Al) atomic layers along the [001] direction (Fig. 1(c)). A coherent interface [4] was assumed between the γ-Ni and γ'-Ni_3Al phases, and thus the lateral lattice parameters for both phases were taken to be the same. Experimental observations have shown that there are ~20 Å thick transition layers between the γ and γ' phases [38], although we used the sandwich model for computational efficiency. The lattices in the sublayer plane were fully relaxed; and the size of the (001) plane was $\sqrt{2}a_0 \times \sqrt{2}a_0$, where a_0 is the lattice constant. The multilayer model was composed of m atomic layers of Ni_3Al (001) and n atomic layers of Ni (001), which means that there were $m/2$ Ni_3Al unit cells and $n/2$ Ni unit cells in the $m(Ni_3Al) + n(Ni)$ multilayer. The (001) γ' atomic layer and (002) γ/γ' atomic layer were regarded as the coherent interface between the Ni and Ni_3Al blocks based on theoretical and experimental results [4,5]. According to previous DFT calculations and experimental studies [26–30], doping at the Al(2) site of the interphase boundary is the most reasonable model. The two alloying atoms were located at Al(2) sites in the (001) γ' atomic layer, as shown in Fig. 1(d), resulting in dopant atom for each (001) γ' plane. This substitution was based on the results of first-principles and experimental site-preference studies [14,39,40]. This process does not consider plastic deformation.

3. Results

3.1. Thickness dependence of the theoretical tensile strength

To check the convergence of the theoretical tensile strength (σ_{max}) versus the thickness of γ-Ni/γ'-Ni_3Al multilayers, four periodic slab models with different thicknesses of $n(Ni) = m(Ni_3Al)$, where n and m = 6, 8, 10, and 12 are the number of atomic layers, were considered in the calculations. The equilibrium configurations were obtained by fully relaxing the slab models, where the tensile test was simulated by gradually stretching the model along the [001] direction while relaxing the (001) plane.

Fig. 2(a) shows the calculated tensile strain energies of γ-Ni/γ'-Ni_3Al multilayers ($\Delta E = E - E_0$) plotted as a function of strain ($\varepsilon = (l - l_0)/l_0$, where l and l_0 are the lengths of the stretched and unstretched states along the [001] direction, respectively) for different slab thicknesses. Here, E is the total energy at the different strain values and E_0 is the total energy in the equilibrium state

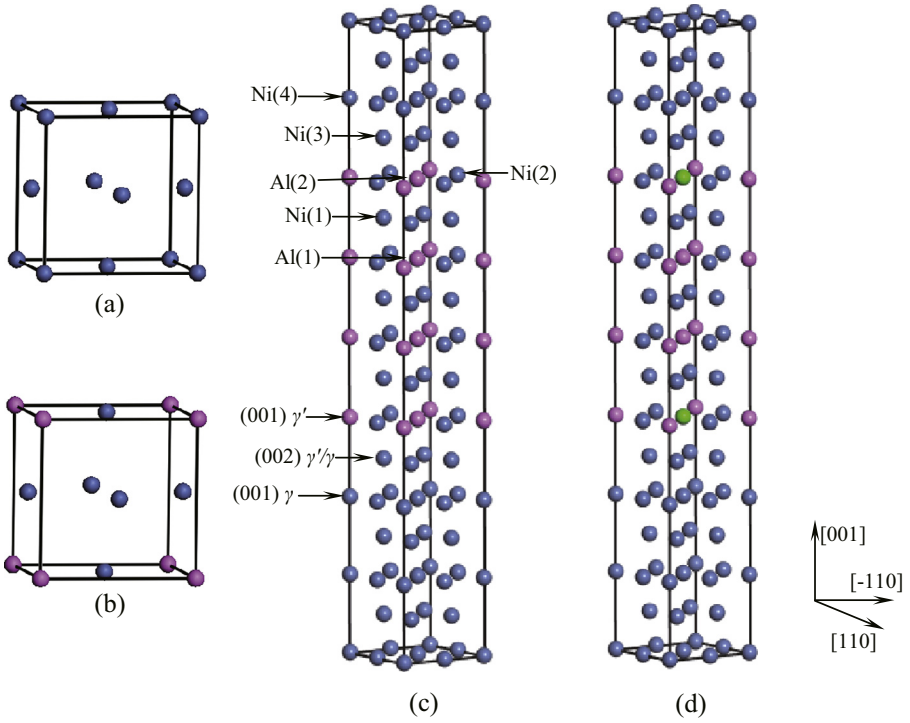

Fig. 1. (a) Conventional unit cell of fcc-Ni, (b) unit cell of $L1_2$-Ni_3Al, (c) periodic repeating blocks of the 8(Ni) + 8(Ni_3Al) multilayer model, and (d) the doped periodic multilayer model. The balls represent Ni (blue), Al (pink), and X (green) atoms, where X = Ta, Cr, Ru, Re, Mo, or W. (For interpretation of the references to color in this figure legend, the reader is referred to the web version of this article.)

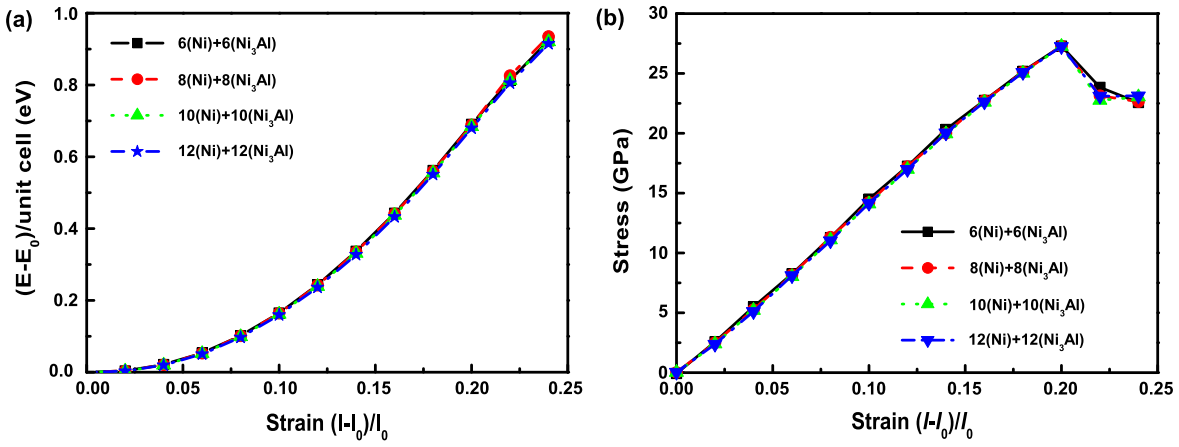

Fig. 2. (a) Energy–strain and (b) stress–strain relationships for different γ-Ni/γ'-Ni_3Al multilayer thicknesses.

($\varepsilon = 0$). The continuous energy–strain curves shown in Fig. 2(a) demonstrate the continuity of the strain path and the reliability of the current method.

The stress–strain curves are plotted in Fig. 2(b), where the tensile stress σ almost linearly increases with increasing strain up to the critical strain value of $\varepsilon_c = \sim 20\%$, where the stress reaches its maximum value and is considered the theoretical tensile strength of the system. The tensile stress then begins to decrease with increasing strain as $\varepsilon > 0.20$. This indicates that the structure of the system becomes unstable. Furthermore, there are only slight differences in both the strain energy and the stress as a function of strain for different thicknesses of the γ-Ni/γ'-Ni_3Al multilayer, as shown in Fig. 2. The calculated lattice constant in the equilibrium state is 3.54 Å. The theoretical tensile strengths are 27.28, 27.28, 27.25, and 27.26 GPa for n(Ni) + n(Ni_3Al) multilayer slab models with n = 6, 8, 10, and 12, respectively (Table 1). This illustrates that the tensile properties are insensitive to the thickness of the γ-Ni/γ'-Ni_3Al multilayer. Therefore, for computational efficiency and to eliminate interaction between dopant atoms, the 8

Table 1
Calculated lateral lattice constants, theoretical tensile strengths, and critical strain values of n(Ni) + n(Ni_3Al) multilayers, where n is the number of atomic layers.

	6(Ni) + 6 (Ni_3Al)	8(Ni) + 8 (Ni_3Al)	10(Ni) + 10 (Ni_3Al)	12(Ni) + 12 (Ni_3Al)
Lateral lattice constant (Å)	3.54	3.54	3.54	3.54
Theoretical tensile strength σ_{max} (GPa)	27.28	27.28	27.25	27.26
Critical strain ε_c	0.20	0.20	0.20	0.20

(Ni) + 8(Ni_3Al) multilayer model was used to investigate the effect of the alloying elements on the tensile properties of the system. For the γ-Ni/γ'-Ni_3Al multilayer model superalloy, the theoretical tensile strength is ~27.28 GPa, which is ~1 GPa higher than that of γ'-Ni_3Al. The critical strain of the superalloy is ~38% lower than the γ'-Ni_3Al phase [24,25], which could be because of the existence of the interface.

3.2. Effect of alloying elements on the theoretical tensile strength of γ-Ni/γ'-Ni_3Al multilayers

To understand the effect of alloying elements on the tensile strength of γ-Ni/γ'-Ni_3Al multilayers, the Al(2) atoms in the two (001) γ' sublayers at the interface of the 8(Ni) + 8(Ni_3Al) multilayer model were replaced by dopant X (X = Re, Ru, W, Ta, Cr, or Mo), as shown in Fig. 1(d). According to recent experiments and density functional theory calculations [14,39,40], the alloying elements Re, Ru, Ta, W, and Mo prefer the Al site in the γ'-Ni_3Al phase, and Co and Cr usually randomly occupy Ni and Al sites. Therefore, we only considered the case of replacement of the Al atoms in the two (001) γ' sublayers at the interface by dopants because the percentage of dopants such as W, Mo, and Re is usually less than ~3 at. %, that is, doping is in the dilute limit. The tensile strengths of γ-Ni/γ'-Ni_3Al multilayers with different dopants were calculated, and the results are shown in Table 2 and Fig. 3. From Table 2, the influence of the alloying elements on the lattice constant is very small (<0.5%), partly because of the small dopant concentration. Except for Ta, all of the dopants in Al sites at the interface improve the tensile properties of the γ-Ni/γ'-Ni_3Al multilayer, including increasing the theoretical tensile strength and critical strain. When the tensile strain is less than 20%, the energy and stress of the system are insensitive to doping. When the tensile strain exceeds ~20%, the different alloying elements have the significantly different effect on the energy and stress of the system.

The stress–strain curves of the different multilayers (inset of Fig. 3(b)) indicate that the W and Re doped alloys have the highest σ_{max} values (8% higher than the undoped alloy), while doping with Mo, Ru, and Cr increases σ_{max} by 7%. However, the Ta dopant has no significant effect on σ_{max}. Alloying also significantly changes ε_c (Table 2). A small amount of Mo or W increases ε_c to 0.24 (20% increase), whereas Re, Ru, and Cr increase ε_c to 0.22 (10% increase). From Fig. 3 and Table 2, it can be concluded that the alloying elements at the interface significantly affects the tensile properties of the γ-Ni/γ'-Ni_3Al multilayer superalloy, and the refractory elements W, Re, and Mo are effective in improving the tensile properties of the superalloy. These results are in agreement with previous computational studies of the ideal tensile strength of the single-phase Ni_3(AlRe) alloy [24]. Nanoindentation measurements of commercial superalloys indicate that their hardness increases with increasing concentration of dopant Re [41]. Three new types of cheap superalloys with high W content have been designed using DFT calculations, and they exhibit superior creep–rupture properties to low W content alloys [42]. Our calculations show that W and Re at the γ-Ni/γ'-Ni_3Al interface have similar effects on the theoretical strength, while W can increase the maximum strain by up to 20%. Thus, we believe that W is the best choice for improving the mechanical properties of Ni-based superalloys. The mechanical properties are closely related to the interactions between atoms, so the electronic origin of the improvement of the tensile properties owing to alloying is discussed in the following section.

4. Discussion

4.1. Local lattice distortion

To understand the effect of doping on the atomic structure of γ-Ni/γ'-Ni_3Al multilayers, the atomic configurations of the multilayer system at different strains (ε = 0%, 10%, 20%, and 24%) are shown in Fig. 4. According to the conventional fcc structure, each atom has 12 first nearest neighbor (1NN) atoms at ε = 0%, where the 1NN atoms of Al(2) are 12 Ni atoms (including Ni(1), Ni(2), Ni(3), and N(4)), and the 1NN atoms of Ni(2) are 8 Al atoms and

Table 2
Calculated lattice constants, longitudinal lengths of the [001] direction, theoretical tensile strengths, and critical strains of doped γ-Ni/γ'-Ni_3Al multilayers.

	Undoped	Ta	Cr	Ru	Re	Mo	W
Lateral lattice constant (Å)	3.54	3.56	3.54	3.54	3.55	3.56	3.56
Longitudinal length (Å)	28.33	28.31	28.20	28.31	28.27	28.27	28.28
Theoretical tensile strength σ_{max} (GPa)	27.282	27.363	29.159	29.317	29.424	29.322	29.433
Critical strain ε_c	0.20	0.20	0.22	0.22	0.22	0.24	0.24

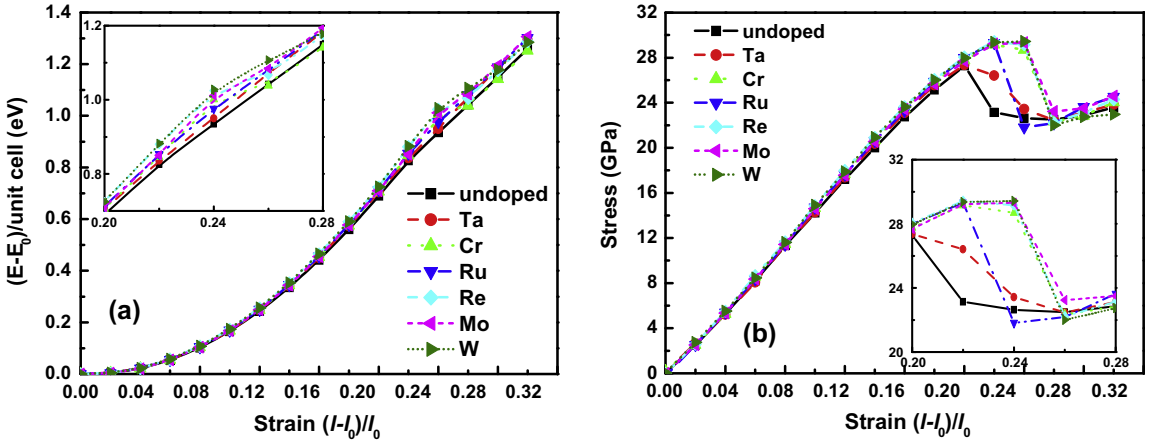

Fig. 3. (a) Energy–strain per unit cell and (b) stress–strain relationships for the different doped Ni(001)/Ni_3Al(001) multilayers. The insets show enlarged plots of the energy and stress in the strain range 0.20–0.28.

4 Ni atoms (including Al(2), Ni(1), and Ni(3)) (Fig. 4(a)). At this strain state, Al(2) and Ni(2) are located in the (001) γ' plane. As the tensile strain increases, the distance between each atomic layer gradually increases and the positions of the atoms relax to balance each strain. However, the atomic arrangement does not change, and there are eight 1NN atoms around both Al(2) and Ni(2) (Fig. 4(b) and (c)). When the tensile strain increases to the critical value of ε_c = 20%, the Ni atomic layer (i.e., Ni(4) atoms) in the γ

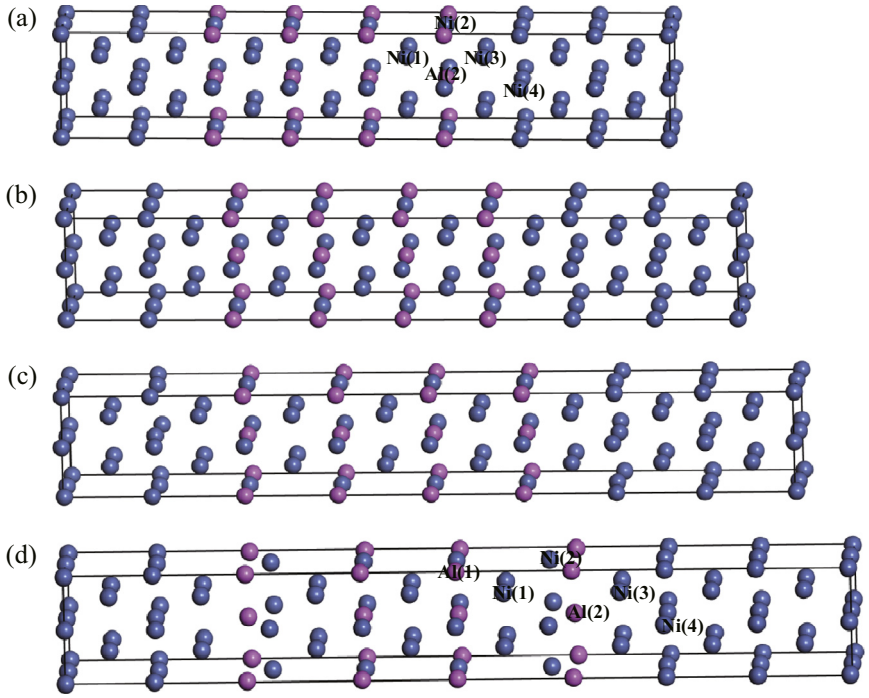

Fig. 4. Local lattice distortion near the interface at the different strain levels: (a) 0%, (b) 10%, (c) 20%, and (d) 24%. The circles represent Ni (blue) and Al (pink) atoms. (For interpretation of the references to color in this figure legend, the reader is referred to the web version of this article.)

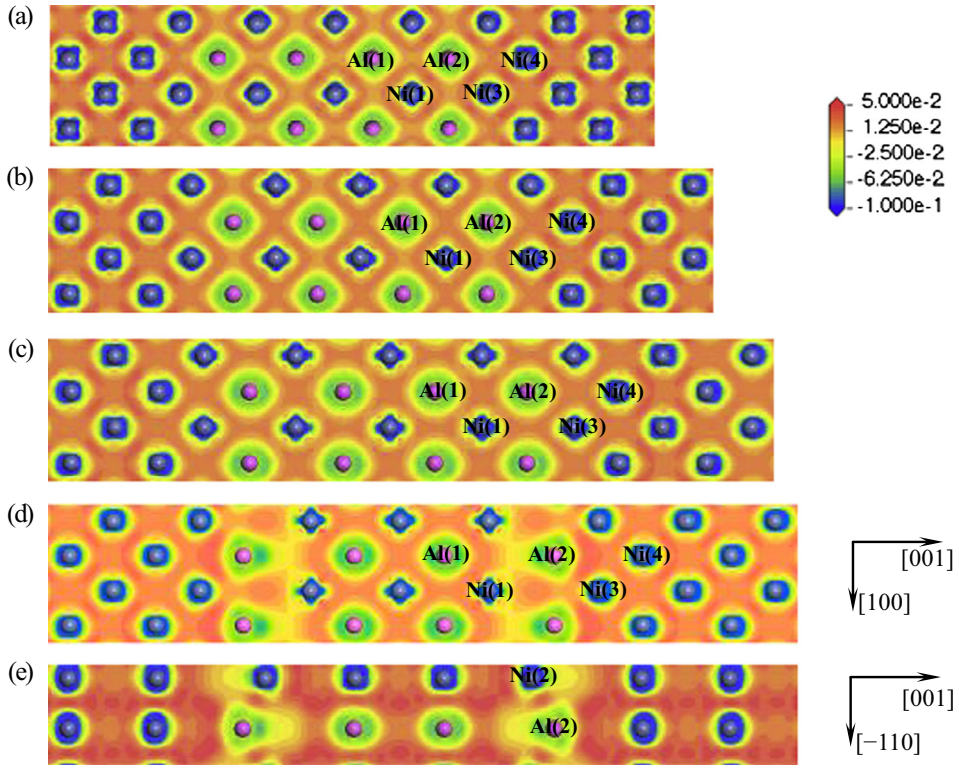

Fig. 5. CDD maps on the (0 1 0) planes of undoped γ-Ni/γ'-Ni_3Al multilayers at strains of (a) 0%, (b) 10%, (c) 20%, and (d) 24%. (e) CDD map on the (1 1 0) plane at 24% strain. Positive (negative) values denote charge accumulation (depletion).

phase adjacent to the interface decomposes, which causes the face-centered Ni atoms to slightly move toward the interface layer (i.e., the Ni(3) atomic layer). However, even though the γ'-Ni_3Al phase is in this high strain state, the Al(2) and Ni(2) atoms are still located in the same (001) γ' atomic layer (Fig. 4(c)). Interestingly, as the tensile strain exceeds the critical value, this γ' atomic layer decomposes into two layers, leading to local atomic rearrangement at the interface. From Fig. 4(d), when the strain reaches 24%, the A1(2) atoms in this layer move toward the interface Ni layer (Ni(3) atomic layer) and the Ni(2) atoms move toward the γ'-Ni_3Al phase. This results in only four Ni(2) atoms being the 1NN atoms of Al(2). The Al–Ni interatomic distance increases to 2.597 Å from the Al–Ni bond length of 2.364 Å in the bulk-like part far from the interface. The Ni(3) atoms become second nearest neighbor (2NN) atoms of

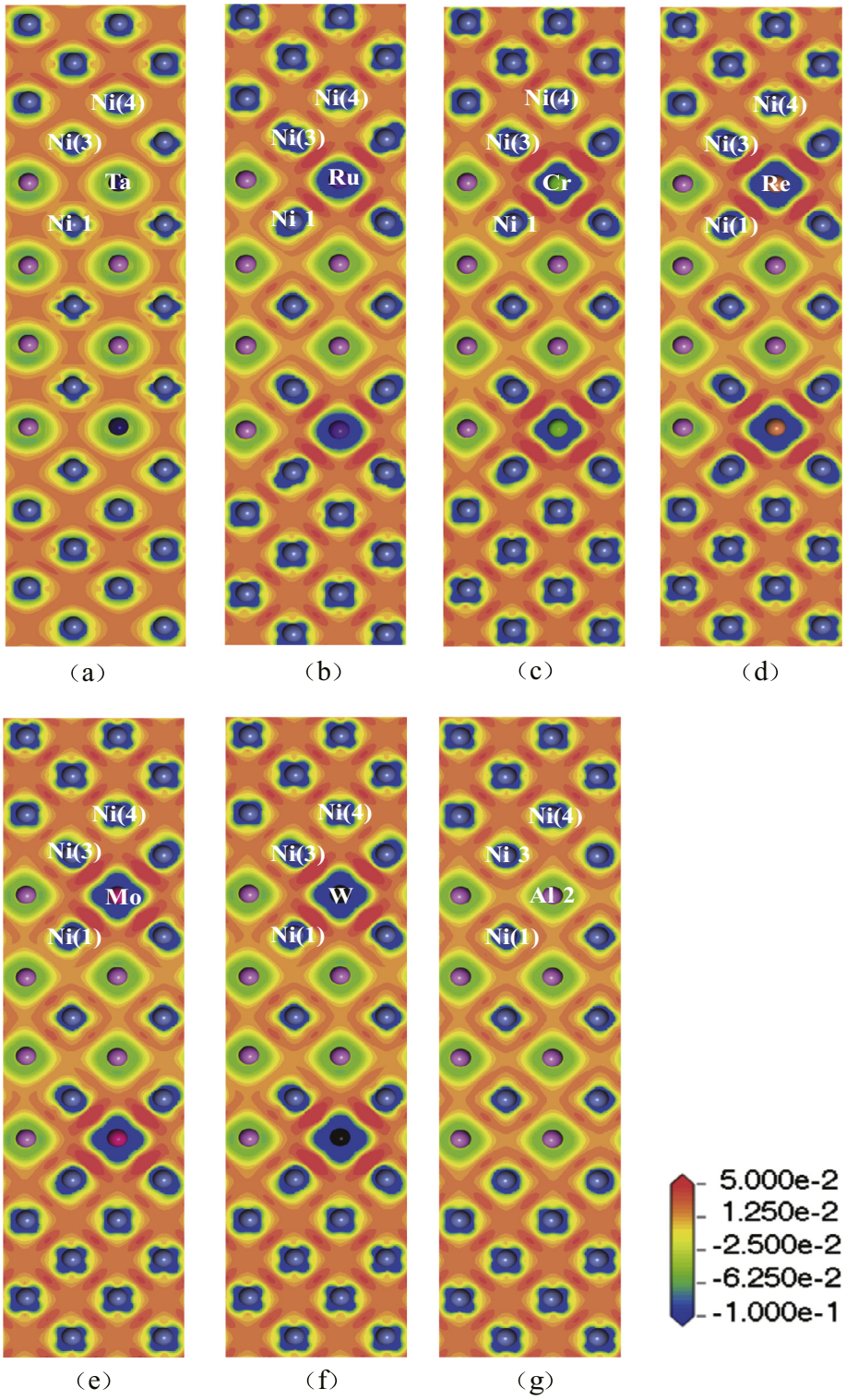

Fig. 6. CDD maps of the (010) planes of γ-Ni/γ'-Ni_3Al multilayers doped with different elements at the initial strain (strain 0%): (a) Ta, (b) Ru, (c) Cr, (d) Re, (e) Mo, and (f) W dopants, and (g) undoped. Positive (negative) values denote charge accumulation (depletion).

Al(2) and the Al–Ni interatomic distance increases to 2.658 Å, while the Ni(1) atoms become third nearest neighbor atoms of Al (2) with an Al–Ni interatomic distance of 3.527 Å. The atomic configuration at high strain, especially close to the critical strain, reveals the bonding characteristics of the alloys. It is worth mentioning that σ_{max} of the γ/γ' multilayer system is 1 GPa higher than that of pure Ni_3Al. However, local atomic disorder occurs at the interface with $\sigma_{max} = 27.28$ GPa and $\varepsilon_c = 0.2$. This indicates that atomic bonding in the γ'-Ni_3Al block should be stronger than the interface bonding. That is, the theoretical tensile strength of the γ'-Ni_3Al block should be higher than 27.28 GPa. The electronic origin of the bonding characteristics is discussed in the following section.

4.2. Electronic structures

To understand the electronic origin of the strengthening effect owing to alloying, the electronic structures of the pure and doped γ-Ni/γ'-Ni_3Al multilayer model systems were analyzed.

The charge-density difference (CDD, $\Delta\rho = \rho - \rho_{free}$, where ρ_{free} is the superposition of the free atomic charge density) maps of the pure and doped γ-Ni/γ'-Ni_3Al multilayers are shown in Figs. 5 and 6. Fig. 5(a)–(c) shows the CDD maps on the (010) plane at strains of $\varepsilon = 0\%$, 10%, and 20%, respectively, and Fig. 5(d) and (e) shows the CDD maps on the (010) and (110) planes at a strain of $\varepsilon = 24\%$. In the unstrained state (Fig. 5(a)), the Ni–Ni bonding in the γ-Ni block far away from the interface exhibits metallic-like character (e.g., see Ni(4) in Fig. 5(a)), whereas the Ni–Al bonding in the γ'-Ni_3Al block exhibits strong covalent-like character. Furthermore, the charge distribution around the Ni atoms at the γ/γ' interface is similar to that of the γ'-Ni_3Al block. As the strain increases, the atomic bonds become longer along the [001] direction and shorter along in the [100] and [010] directions, leading to charge redistribution.

As the strain increases, the charge distribution become increasingly sparse, indicating that interactions between atoms become weaker, especially along the [001] direction (Fig. 5(b) and (c)). When the strain reaches 20%, the charge density between atoms greatly decreases and charge distribution around Al atoms evolves into an elliptical shape (Fig. 5(c)) rather than the square cross-section in the initial state (Fig. 5(a)). This indicates that at a strain of 20%, interactions between atoms and the directional bonds between Al and Ni are weak. As evidenced by the above discussion, the tensile stress reaches its maximum value at a strain of 20% and the system becomes unstable when the strain exceeds this threshold value. To investigate the deformation characteristics of the material, charge redistribution of the (010) (Fig. 5(d)) and (110) (Fig. 5(e)) planes at a strain of 24% was investigated. As shown in Fig. 5(d), the charge distribution between Al(2) and Ni(1) is very sparse in the (010) plane. This is the result of Ni(1) atoms being 2NN atoms of Al(2), and Ni(2) atoms being 1NN atoms, as discussed in Section 4.1. However, the charge distribution in the (110) plane is denser between Al(2) and Ni(3) than between Al (2) and Ni(2), which can be seen by comparing Fig. 5(d) and (e). This higher density between Al(2) and Ni(3) means more charge transfer to the Al(2)–Ni(3) bond and a stronger interaction between Al(2) and Ni(3) than between Al(2) and the 1NN Ni(2). Therefore, local atomic rearrangement would occur in (001) γ'.

Fig. 6 shows CDD maps of the (010) planes of the doped γ-Ni/γ'-Ni_3Al multilayers at the initial strain, which show charge redistribution owing to doping. The CDD map of the undoped multilayer is shown in Fig. 6(g) for comparison. More electrons accumulate between X (X = Re, W, Mo, Ru, and Cr) and its 1NN Ni atoms than in the undoped multilayer, but there is no obvious accumulation of

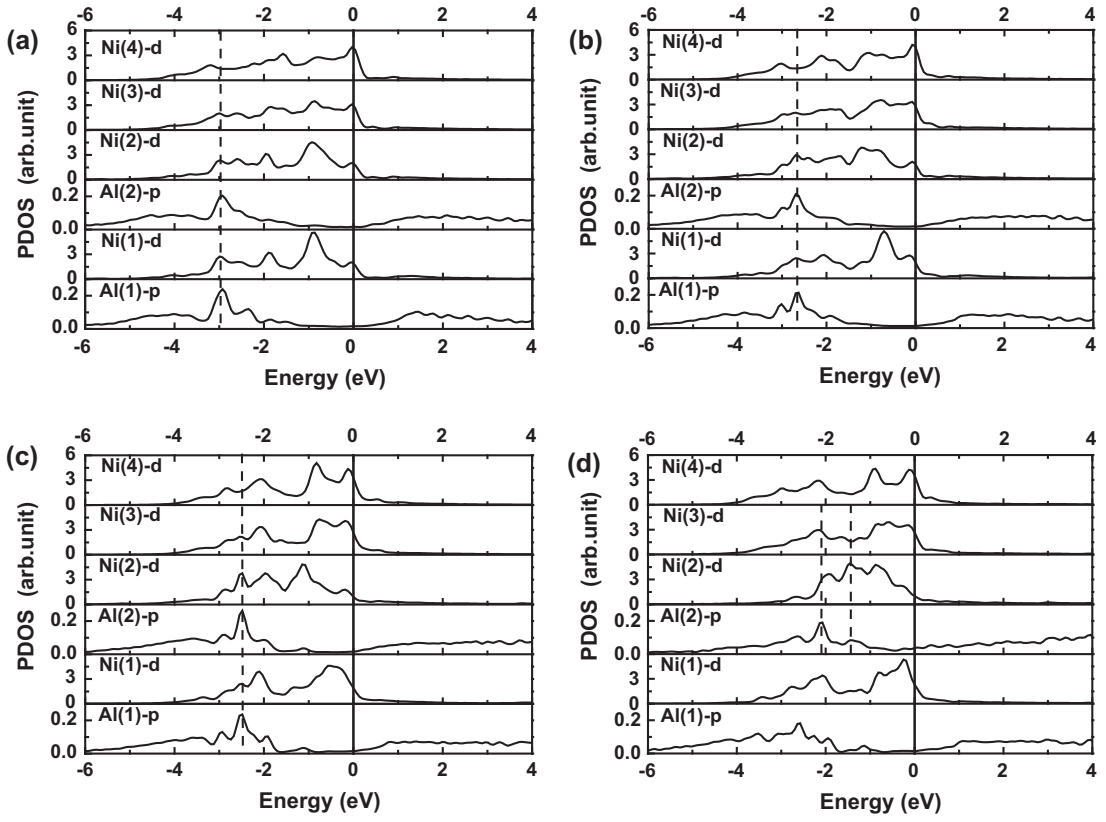

Fig. 7. PDOS of different atoms in the undoped γ-Ni/γ'-Ni_3Al multilayer at strains of (a) 0%, (b) 10%, (c) 20%, and (d) 24%. The Fermi energy level is shifted to zero.

electrons around Ta. This indicates that bonding of Re, W, Mo, Ru, and Cr and their 1NN Ni atoms in the doped γ-Ni/γ'-Ni_3Al multilayers is stronger than Al–Ni bonding in the undoped γ-Ni/γ'-Ni_3Al multilayer. Additionally, the bonding characteristics of the dopant atoms and their 1NN atoms are strongly correlated with the improved mechanical properties of the systems. The bonding characteristics of the dopant atoms and their 1NN Ni atoms can be determined by analyzing the shape of the charge correlation region of the dopant atom. The Cr–Ni, Re–Ni, Mo–Ni, and W–Ni bonds are highly directional (Fig. 6(c)–(f)), which indicates covalent-like character. This covalent-like bonding will resist tensile deformation, leading to higher strength. In contrast, charge accumulation around Ta and Ru is mainly spherically symmetric, which indicates metallic bonding (Fig. 6(a) and (b)). The improvement in the tensile strength with the addition of Ru is less than with the addition of Re, W, and Mo.

In addition to the CDD, the partial density of states (PDOS) was analyzed to gain further insight into changes in the chemical bonds and charge distribution during the tensile straining process. Fig. 7 shows the PDOS of Ni and Al at the different strains states, which display the p valence electron distributions of Al(1) and Al(2) atoms and the d valence electron distributions of Ni(1), Ni(2), Ni(3), and Ni(4) atoms in the energy space. Hybridization of the Al-p and Ni-d bands determines the bonding of Ni_3Al ordered alloys. In the unstrained state (Fig. 7(a)), there are few Al-p electronic states at the Fermi level and broad overlap between the Al-p and Ni-d valence electrons between $[-5, 0]$ eV. This indicates weak metallic bonding and strong covalent-like bonding between 1NN Ni and Al atoms in the γ'-Ni_3Al block and at the interface. In addition, the PDOS of Al(1), Al(2), Ni(1), Ni(2), and Ni(3) atoms share an overlapping peak near -3 eV, indicating hybridization of Al-p and Ni-d bands, which plays a deterministic role in interface adhesion. This overlapping peak moves higher energy as the strain increases. It is located at -2.7 eV with 10% strain (Fig. 7(b)) and at -2.5 eV with 20% strain (Fig. 7(c)), which shows that the Al–Ni bond becomes weak owing to deformation. When $\varepsilon = 24\%$, the Al(2) and Ni(2) atoms share an overlapping peak near -1.5 eV, and the Al(2) and Ni(3) atoms share an overlapping peak near -2.1 eV (Fig. 7(d)). This indicates that the bonding between Al(2) and Ni(3) is stronger than that between Al(2) and Ni(2), which is consistent with the analysis of the stress–strain relation and the CDD.

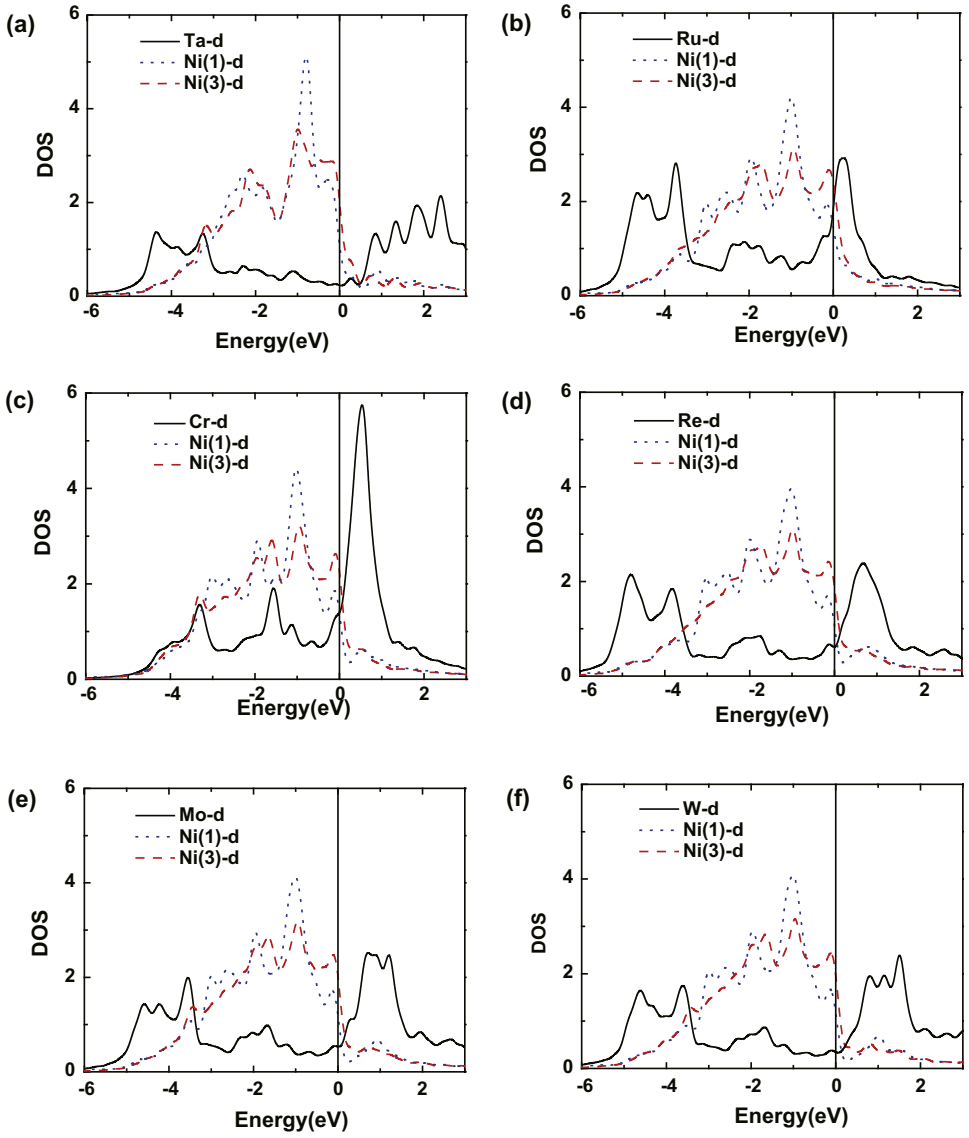

Fig. 8. PDOS for different dopants and their 1NN Ni atoms in the γ-Ni/γ'-Ni_3Al multilayer at the initial strain (strain 0%): (a) Ta, (b) Ru, (c) Cr, (d) Re, (e) Mo, and (f) W dopant atoms. The Fermi energy level is shifted to zero.

To gain further insight into the bonding between Ni and Al atoms in the γ'-Ni_3Al block of the superalloy, we carried out a Bader charge analysis [43]. The predicted Bader charges of Ni and Al in single-phase γ'-Ni_3Al are 10.602*e* and 1.198*e*, respectively, and the charge of Ni in single-phase γ-Ni is 10*e*. Interestingly, the Bader charge of Ni in the γ'-Ni_3Al block of the multilayered model is at least 0.01*e* and up to 0.06*e* higher than that of the single γ'-Ni_3Al phase. The charge of Al decreases by at least 0.07*e*, and the average decrease of the Al charge is 0.087*e*. The Bader charge of Ni in the γ-Ni phase does not significantly change. These findings indicate that transformation of γ'-Ni_3Al to γ-Ni could lead to further charge transfer from Al to Ni in the γ'-Ni_3Al block. Charge redistribution in the γ'-Ni_3Al block strengthens electrostatic interactions, and thus bonding between Ni and Al. This result can be used to understand the increased theoretical strength of both the multilayer superalloy (Section 3.1) and γ'-Ni_3Al block.

Because the narrow d-band governs the bonding characteristics of transition metals [44–46], the site projected d-DOS of the alloying elements in the doped γ-Ni/γ'-Ni_3Al multilayers were calculated (Fig. 8(a)–(f)). The d-DOS of the 1NN Ni atoms of the X dopants are also plotted in each figure to estimate the bonding characteristic. From Fig. 8(c)–(f), the Fermi energy levels with Cr, Re, W, and Mo dopants are located in the pseudogap, which separates the bonding and antibonding states of the PDOS for dopants. These show covalent-like bonding character, which indicates a strong bond between the dopant and the host Ni atom. In contrast, the Fermi energy level penetrates the PDOS peak for Ta and Ru (Fig. 8(a) and (b)), which is a PDOS feature that is closely related to metallic bonding. This is why Ta and Ru substitution for the Al (2) atom does not significantly improve the tensile strength of the system. Comparing the site projected d-DOS of Ni(1) and Ni (3) with the PDOS of the dopants, X atoms (except for Ta and Ru) are more prone to undergo d–d hybridization with Ni(3) atoms. For instance, Cr and Ni(3) share two d-DOS peaks at about −1.7 and −3.4 eV, whereas Re, Mo, and W have a broad DOS peak between about −2.7 and −1 eV, which partially overlaps with the d-DOS of both Ni(1) and Ni(3). Conversely, both Ni(1) and Ni(3) atoms share a DOS peak just below the Fermi level, indicating that this additional d–d hybridization would strengthen interface adhesion. The DOS analysis indicates that the NiAlX atomic layer decomposes into two atomic planes, the Al–X plane move toward the γ-Ni block, and the Ni atomic plane moves toward the γ'-Ni_3Al block. Therefore, we suggest that the additional d–d hybridization of Ni(1)–X should account for the increase of the ideal tensile strength of the γ-Ni/γ'-Ni_3Al superalloy owing to alloying.

The PDOS analysis is consistent with the CDD analysis, and these electronic structures provide important information about how doping affects the theoretical tensile strength of Ni-based superalloys.

5. Conclusions

The theoretical tensile strength of Ni-based superalloys has been investigated by DFT calculations. The superalloy was modeled as a γ-Ni/γ'-Ni_3Al multilayer. The strengthening effect of doping Re, Ru, Cr, Mo, W, or Ta close to the γ/γ' interface was investigated. Theoretical calculations show that the tensile strength of the superalloy is 27.28 GPa in the [001] direction at a critical strain of 0.20, which is about 1 GPa higher than that of the γ'-Ni_3Al phase. However, the critical strain of the multilayer system is ~38% lower than that of a pure γ'-Ni_3Al phase. Except for Ta, doping at the Al site of the γ-Ni/γ'-Ni_3Al interface significantly increases the theoretical tensile strength or the maximum strain of the γ-Ni/γ'-Ni_3Al multilayer. The refractory elements Cr, W, Re, Ru, and Mo increase σ_{max} by more than ~7%. Cr, Re, and Ru increase ε_c by about 10%, while Mo and W can increase ε_c up to 20%. Local lattice analysis of the undoped γ-Ni/γ'-Ni_3Al multilayer at different strains shows that local atomic disorder would occur in the Ni–Al sublayer of the γ'-Ni_3Al block, wherein the Ni–Al atomic layer decomposes into an Al layer and a Ni layer when the strain exceeds a critical value. Bader charge analysis indicates that precipitation of γ'-Ni_3Al into γ-Ni could lead to charge transfer from Al to Ni in the γ'-phase, and thus increase the theoretical strength of the γ'-block and the superalloy. Analysis of the CDD and PDOS provides further insight into changes in the chemical bonds and charge redistribution during the tensile process. Moreover, covalent-like Ni–X bonds effectively inhibit deformation of the system and lead to tensile strengthening in doped γ-Ni/γ'-Ni_3Al multilayers. The additional d–d hybridization of Ni(1)–X accounts for the increase of the ideal tensile strength of Ni-based superalloys owing to doping.

Acknowledgments

This work was supported by the "973 Project" from the Ministry of Science and Technology of China (Grant No. 2011CB606402), the National Natural Science Foundation of China (Grant No. 51071091), and the Innovation Funds of the Inner Mongolia University of Science and Technology (2010NC059). The calculations were performed using the "Explorer 100" cluster system at the Tsinghua National Laboratory for Information Science and Technology in Beijing, China.

References

[1] R.C. Reed, The Superalloys: Fundamentals and Applications, Cambridge University Press, Cambridge, UK, 2006.
[2] T.M. Pollock, S. Tin, J. Propul. Power 22 (2006) 361.
[3] H.K.D.H. Bhadeshia, Nickel Based Superalloys, The website of University of Cambridge, <http://www.msm.cam.ac.uk/phase-trans/2003/Superalloys/superalloys.html>.
[4] C. Wang, C.Y. Wang, App. Surf. Sci. 255 (2009) 3669.
[5] H. Harada, A. Ishida, H.K.D.H. Bhadeshia, M. Yamazaki, Appl. Surf. Sci. 67 (1993) 299.
[6] T.M. Pollock, A.S. Argon, Acta Metall. Mater. 42 (1994) 1859.
[7] A. Epishin, T. Link, P.D. Portella, U. Brückner, Acta Mater. 48 (2000) 1981.
[8] D.D. Pearson, F.D. Lemkey, B.H. Kear, Superalloys, in: J.K. Tien, S.T. Wlodek, H. Morrow, M. Gell, G.E. Maurer (Eds.), The Minerals, Metals & Materials Society, ASM, Metals Park, OH, 1980, pp. 513–519.
[9] H. Harada, K. Ohno, T. Yamagata, T. Yokokawa, M. Yamazaki, Superalloys, in: S. Reichman, D.N. Duhl, G. Maurer, S. Antolovich, C. Lund (Eds.), The Minerals, Metals & Materials Society, Warrendale, PA, 1988, pp. 733–741.
[10] J.K. Tien, R.P. Gamble, Metall. Trans. 3 (1972) 2157.
[11] R. Srinivasan, R. Banerjee, J.Y. Hwang, Phys. Rev. Lett. 102 (2009) 086101.
[12] K. Chen, L.R. Zhao, J.S. Tse, Mater. Sci. Eng. A 360 (2003) 197.
[13] S. He, P. Peng, L. Peng, Y. Chen, H. Wei, Z.Q. Hu, J. Alloy. Compd. 597 (2014) 243.
[14] X.X. Yu, C.Y. Wang, X.N. Zhang, P. Yan, Z. Zhang, J. Alloy. Compd. 582 (2014) 299.
[15] X.X. Yu, C.Y. Wang, Mater. Sci. Eng. A 539 (2012) 38.
[16] Z.G. Liu, C.Y. Wang, T. Yu, Comput. Mater. Sci. 83 (2014) 196.
[17] M. Yoshida, T. Sumomogi, T. Endo, H. Maeta, T. Kino, Mater. Trans. 48 (2007) 1.
[18] D. Lorenz, A. Zeckzer, U. Hilpert, P. Grau, H. Johansen, H.S. Leipner, Phys. Rev. B 67 (2003) 172101.
[19] A. Gouldstone, N. Chollacoop, M. Dao, J. Li, A.M. Minor, Y.L. Shen, Acta Mater. 55 (2007) 4015.
[20] X. Huang, N. Hansen, N. Tsuji, Science 312 (2006) 249.
[21] A.M. Iskandarov, S.V. Dmitriev, Y. Umeno, Phys. Rev. B 84 (2011) 224118.
[22] S. Ogata, J. Li, N. Hirosaki, Y. Shibutani, S. Yip, Phys. Rev. B 70 (2004) 104104.
[23] Y.L. Liu, Y. Zhang, H.B. Zhou, G.H. Lu, M. Kohyama, J. Phys.: Condens. Matter 20 (2008) 335216.
[24] Y.J. Wang, C.Y. Wang, Scripta Mater. 61 (2009) 197.
[25] Y.J. Wang, C.Y. Wang, Appl. Phys. Lett. 94 (2009) 261909.
[26] X.F. Gong, G.X. Yang, Y.H. Fu, Y.Q. Xie, J. Zhuang, X.J. Ning, Comput. Mater. Sci. 47 (2009) 320.
[27] K. Chen, L.R. Zhao, J.S. Tse, Acta Mater. 51 (2003) 1079.
[28] K. Chen, L.R. Zhao, J.S. Tse, Philos. Mag. 83 (2003) 1685.
[29] K. Chen, L.R. Zhao, J.S. Tse, Mater. Sci. Eng. A 365 (2004) 80.
[30] L. Peng, P. Peng, Y.G. Liu, S. He, H. Wei, T. Jin, Z.Q. Hu, Comput. Mater. Sci. 63 (2012) 292.
[31] P. Peng, D.W. Zhou, J.S. Liu, R. Yang, Z.Q. Hu, Mater. Sci. Eng. A 416 (2006) 169.

[32] L. Peng, P. Peng, D.D. Wen, Y.G. Liu, H. Wei, X.F. Sun, Z.Q. Hu, Model. Simul. Mater. Sci. Eng. 19 (2011) 065002.
[33] D. Roundy, C.R. Krenn, M.L. Cohen, Phys. Rev. Lett. 82 (1999) 2713.
[34] D. Roundy, C.R. Krenn, M.L. Cohen, Philos. Mag. A 81 (2001) 1725.
[35] G. Kresse, M. Marsman, J. Furthmüller, VASP the Guide, <http://cms.mpi.univie.ac.at/vasp>.
[36] P.E. Blochl, Phys. Rev. B 50 (1994) 17953.
[37] J.P. Perdew, K. Burke, M. Ernzerhof, Phys. Rev. Lett. 77 (1996) 3865.
[38] H.J. Monkhorst, J.D. Pack, Phys. Rev. B 13 (1976) 5188.
[39] S.Y. Wang, C.Y. Wang, J.H. Sun, W.H. Duan, D.L. Zhao, Phys. Rev. B 65 (2001) 035101.
[40] Y. Zhou, Z.G. Mao, C. Booth-Morrison, D.N. Seidman, Appl. Phys. Lett. 93 (2008) 171905.
[41] K. Durst, O. Franke, M. Göken, Superalloys, in: K.A. Green, T.M. Pollock, H. Harada, T.E. Howson, R.C. Reed, J.J. Schirra, S. Walston (Eds.), The Minerals, Metals & Materials Society, 2004, pp. 467–890.
[42] I.M. Razumovskii, A.V. Ruban, V.I. Razumovskiy, Mater. Sci. Eng. A 497 (2008) 18.
[43] R.F. Bader, Atoms in Molecules – A Quantum Theory, Oxford University Press, Oxford, UK, 1990.
[44] D.G. Pettifor, Solid State Phys. 40 (1987) 43.
[45] W.A. Harrison, Electronic Structure and the Properties of Solids: The Physics of the Chemical Bond, second ed., Dover, New York, USA, 1989.
[46] J. Friedel, M.J. Ziman (Eds.), The Physics of Metals: 1. Electrons, Cambridge University Press, London, UK, 1969 (Chapter 8).